

# Modeling and Simulation of Vehicle Dynamics on the Surface of Phobos<sup>1</sup>

Marco B. Quadrelli<sup>2</sup>, J. (Bob) Balaram<sup>3</sup>, Abhinandan Jain<sup>4</sup>, Jonathan Cameron<sup>5</sup>, Steven Myint<sup>6</sup>, Avinash Devalla<sup>7</sup>

*Jet Propulsion Laboratory, California Institute of Technology  
4800 Oak Grove Drive, Pasadena, CA 91109-8099*

In this paper we analyze the dynamics of a spacecraft in proximity of Phobos by developing the equations of motion of a test mass in the Phobos rotating frame using a model based on circularly-restricted three body problem, and by analyzing the dynamics of a ATHLETE hopper vehicle interacting with the soil under different soil-interaction conditions. The main conclusion of the numerical studies is that the system response is dominated by the stiffness and damping parameters of the leg springs, with the soil characteristics having a much smaller effect. The system simulations identify ranges of parameters for which the vehicle emerges stably (relying only on the passive viscoelastic damper at each leg) or unstably (needing active attitude control) from the hop. The implication is that further experimental and possibly computational modeling work, as well as site characterization (from precursor missions) will be necessary to obtain validated performance models.

## Nomenclature

$\mathbf{a}_{J_2}$ ,  $\mathbf{a}_{J_3}$ ,  $\mathbf{a}_{gyro}$ ,  $\mathbf{a}_{3rd}$  = acceleration vectors

$G$  = shear strength

$V_{rel}$  = relative tangential velocity at the point of contact

$\mathbf{R}_0$  = vector of the position of the test mass with respect to the origin of the Phobos-centric frame

$F_n$  = normal force

$F_t$  = tangential force

$S$  = contact area

$c$  = soil cohesion parameter

$j$  = tangential penetration

$K$ ,  $k_c$  and  $k_\phi$  = soil parameters from [Zhou]

$\rho$  = soil density

$\nu$  = soil Poisson's ratio

$\mu_{Phobos}$  = Phobos gravitational parameter

$\mu_{Mars}$  = Mars gravitational parameter

$\omega$  = angular velocity of the rotating frame

$\delta$  = soil penetration depth

$\mu$  = Coulomb friction coefficient

$\sigma$  = normal stress

$\tau$  = tangential stress

$\phi$  = soil angle of friction

---

<sup>1</sup> © 2015 California Institute of Technology. Government sponsorship acknowledged. This research was carried out at the Jet Propulsion Laboratory, California Institute of Technology, under a contract with the National Aeronautic and Space Administration.

<sup>2</sup> Corresponding author, Research Technologist, Mobility and Robotic Systems Section, Mail Stop 198-219, AIAA Associate Fellow.

<sup>3</sup> Mobility and Robotic Systems Section, Mail Stop 198-219.

<sup>4</sup> Mobility and Robotic Systems Section, Mail Stop 198-219.

<sup>5</sup> Mobility and Robotic Systems Section, Mail Stop 198-219.

<sup>6</sup> Mobility and Robotic Systems Section, Mail Stop 198-219.

<sup>7</sup> Graduate Student, University of Michigan.

## I. Introduction

THIS paper describes recent work done in modeling and simulation of vehicle dynamics on the surface of Phobos. This effort is part of a larger systems engineering capability developed at JPL to answer key questions, validate requirements, conduct key system and mission trades, and evaluate performance and risk related to small body operations for any proposed human or robotic missions to a asteroids and small bodies [Balaram et al.]. As a precursor to landing a human on Mars, NASA is interested in developing a capability to deliver humans, performing experiments, and then returning safely from the surface of Phobos. The study focused on three aspects of the problem: a) Orbital dynamics near the surface; b) Modeling of the interaction between the footpad and regolith material, and c) Analysis of system level effects relating to the hopper configuration geometry.

## II. Concept of operations near surface

Certain periods of a mission to Phobos would require the spacecraft to remain stationary relative to Phobos. Phobos is characterized by its close proximity to Mars, leading to a strong tidal effect. Its irregular shape leads to a complex gravity field on the surface. Its relatively fast rotation leads to a considerable centrifugal effect on the surface. Phobos is a dark body that appears to be composed of C-type surface materials. It is similar to the C-type (blackish carbonaceous chondrite) asteroids that exist in the outer asteroid belt. The regolith layer at Phobos is 20 to 120 m thick in most places, and less than 10 meters in Stickney region. The soil properties are poorly known but it is believed that the upper limit on grain size is ~10-100 microns. There is also evidence for surface particle transport with topography and influenced by Mars tidal pattern [Castillo]. Finally, particle friction and electrostatic charging are difficult to model, but are believed to play an important role in the regolith properties. More details can be found in [Davis et al., Dobrowolskis et al., Duxbury, Thomas et al.]

The particular hopper model and configuration was based on an ATHLETE-derived mechanical configuration with springs and footpads in place of wheels (courtesy of Scott Howe, JPL). The Phobos hopper would use actuated springs – the spring could be compressed passively due to impact or actively due to the electrically powered actuator. A mechanical ratchet mechanism would keep the spring compressed until the ratchet is released. The kinetic energy during descent to Phobos surface would be conserved when the springs are compressed on impact, converting to potential energy in the spring. The potential energy stored in the spring could either be immediately released in a “hop”, partially or controlled released to “hop” in a specified direction, or ratcheted down to be released later. In this scenario, energy losses would occur due to buckling, actuator mechanism, and some losses during impact. These losses would be recuperated each time the hopper would impact the ground by adding compression to the spring through an actuator electrical current (how much depends on the eventual design of the mechanism), thrusting downwards using propellant during landing to help compress the spring, or using ATHLETE motors to push down at the right instant and compress the spring. The release of the compressed spring would thrust the vehicle upward and would convert to kinetic energy and gravitational potential energy. Figure 1 shows the elements considered in this paper for the modeling and simulation of the vehicle surface operations, and a block diagram showing the functions that would be involved in this concept. Figure 2 shows the functional diagram of the iterative modeling and simulation process used for the analysis of vehicle locomotion on Phobos.

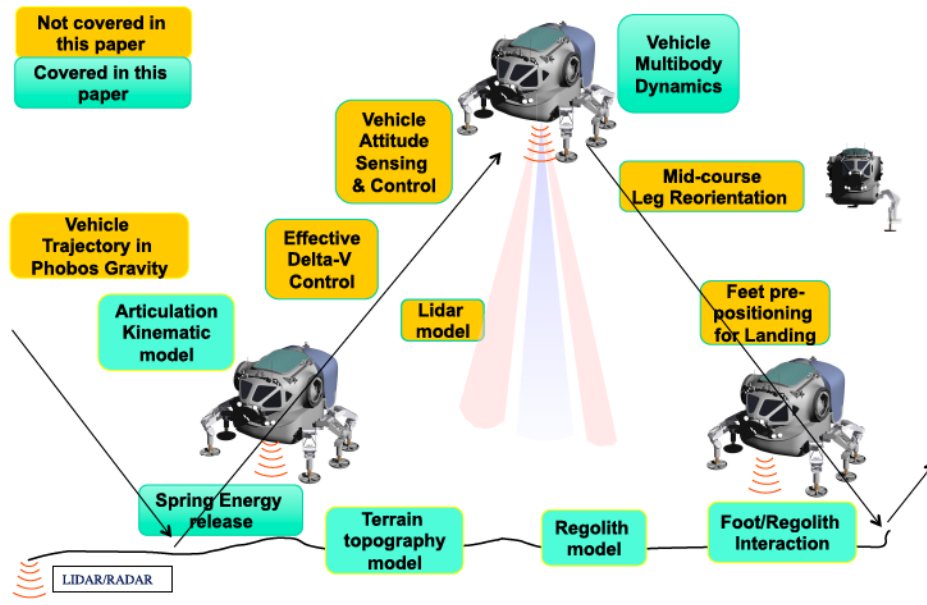


Figure 1. Modeling and Simulation of Hopping Process.

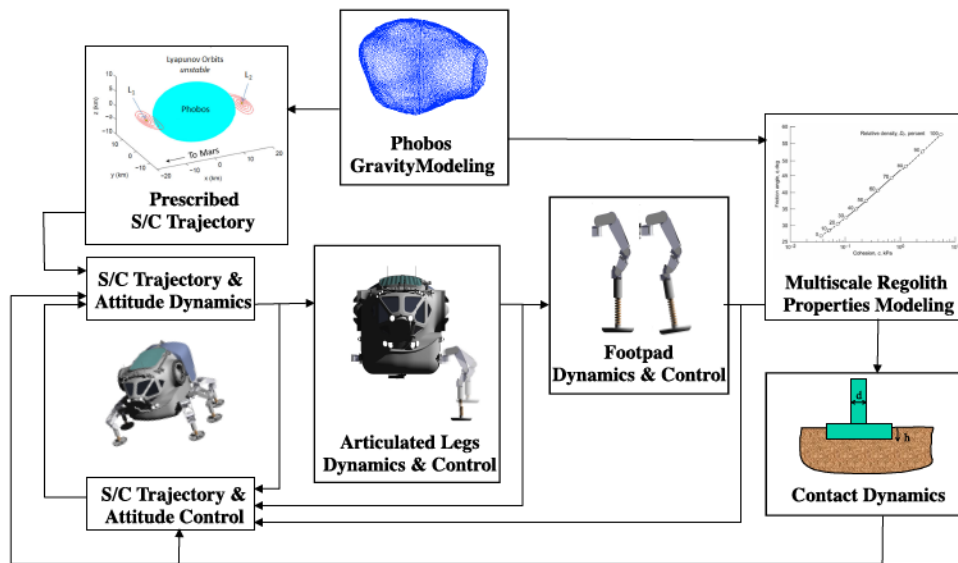


Figure 2. Iterative Modeling of Locomotion on Phobos.

Thrusters could prolong or direct the “hop” motion until kinetic energy reaches zero at the highest altitude and gravitational potential energy is at its peak, whereupon the hopper would fall to the surface again and the “hop” cycle repeats. Since the ATHLETE limbs are articulated, a LIDAR system could constantly monitor the target landing area to create high fidelity 3D models and would “aim” each of the six legs to land at exactly the same time the instant of impact. The forward momentum could be conserved by releasing the springs sequentially (presumably from the back to the front), and continuing the hop in the desired direction. The ATHLETE limbs would not need to land or take off with the springs perfectly vertical: any variation or angle would also be allowed that will provide a more efficient landing or take-off stance, and could be modified “mid-stride”. The hopper could use reaction wheels to keep the vehicle parallel to the surface. The propellant would be limited, but electrical power could be recharged and used over and over again. The ATHLETE legs are modular, and each ATHLETE leg would have a tool adapter at the end. Mars surface mobility wheels, and Phobos hopper springs, are both interchangeable tools that could be

used for this purpose. The hopper vehicle would be fitted with springs for Phobos mobility and, after the Phobos exploration phase, the same vehicle would be taken down to Mars surface, where the springs would be changed with wheels. The ATHLETE legs would be highly articulated, and would be designed to provide active suspension and compliance.

### III. Orbital dynamics near surface

The simulations have been carried out within the assumption of the circularly-restricted three-body problem. The equations of motion of a unit mass close to surface of Phobos, in the Mars-Phobos rotating frame, are:

$$\begin{aligned}
\mathbf{V}_0 &= \dot{\mathbf{R}}_0 \\
\dot{\mathbf{V}}_0 &= -\frac{\mu_{Phobos}}{|\mathbf{R}_0|^3} \mathbf{R}_0 + \mathbf{a}_{J_2} + \mathbf{a}_{J_3} + \mathbf{a}_{3rd} + \mathbf{a}_{gyro} \\
\mathbf{a}_{gyro} &= -\omega \times \omega \times \mathbf{R}_0 - 2\omega \times \dot{\mathbf{R}}_0 \\
\mathbf{a}_{J_2} &= \frac{3}{2} \frac{\mu_{Phobos} J_2}{|\mathbf{R}_0|^5} \begin{bmatrix} x \left( 1 - 5 \frac{z^2}{|\mathbf{R}_0|^2} \right) & y \left( 1 - 5 \frac{z^2}{|\mathbf{R}_0|^2} \right) & z \left( 3 - 5 \frac{z^2}{|\mathbf{R}_0|^2} \right) \end{bmatrix} F_I \\
\mathbf{a}_{J_3} &= \frac{5}{2} \frac{\mu_{Phobos} J_3}{|\mathbf{R}_0|^6} \begin{bmatrix} x \left( 3 - 7 \frac{z^2}{|\mathbf{R}_0|^2} \right) \frac{z}{|\mathbf{R}_0|} & y \left( 3 - 7 \frac{z^2}{|\mathbf{R}_0|^2} \right) \frac{z}{|\mathbf{R}_0|} & z \left( 6 - 7 \frac{z^2}{|\mathbf{R}_0|^2} \right) \frac{z}{|\mathbf{R}_0|} - 3|\mathbf{R}_0|/5 \end{bmatrix} F_I \\
\mathbf{a}_{3rd} &= \mu_{Mars} \left( \frac{(\mathbf{r}_{Mars} - \mathbf{R}_0)}{|\mathbf{r}_{Mars} - \mathbf{R}_0|^3} - \frac{\mathbf{r}_{Mars}}{|\mathbf{r}_{Mars}|^3} \right) + (\mathbf{a}_{J_2} + \mathbf{a}_{J_3})_{Mars}
\end{aligned} \tag{1}$$

where  $\mu_{Phobos}$  is the Phobos gravitational parameter,  $\mu_{Mars}$  is the Mars gravitational parameter,  $\omega$  is the angular velocity of the rotating frame,  $\mathbf{R}_0$  is the vector of the position of the test mass with respect to the origin of the Phobos-centric frame (with components  $x, y, z$ ),  $\mathbf{a}_{J_2}$ ,  $\mathbf{a}_{J_3}$ ,  $\mathbf{a}_{gyro}$ ,  $\mathbf{a}_{3rd}$  are the acceleration vector of the test mass due to Phobos J2 and J3 gravitational harmonics, the Coriolis and centrifugal acceleration due to the motion of the rotating frame, and the Mars third-body acceleration.

		Longitude [deg]											
		0	30	60	90	120	150	180	210	240	270	300	330
Latitude [deg]	-90	0.3616	0.3616	0.3616	0.3616	0.3616	0.3616	0.3616	0.3616	0.3616	0.3616	0.3616	0.3616
	-60	0.4397	0.4484	0.4604	0.4648	0.4584	0.4483	0.4450	0.4518	0.4610	0.4626	0.4539	0.4426
	-30	0.5103	0.5472	0.6088	0.6378	0.6137	0.5614	0.5359	0.5669	0.6181	0.6362	0.6014	0.5395
	0	0.5099	0.5633	0.6586	0.7058	0.6734	0.5933	0.5480	0.5933	0.6734	0.7058	0.6586	0.5633
	+30	0.4949	0.5241	0.5859	0.6206	0.6027	0.5515	0.5204	0.5459	0.5981	0.6223	0.5935	0.5319
	+60	0.4430	0.4470	0.4605	0.4705	0.4684	0.4577	0.4500	0.4542	0.4658	0.4727	0.4670	0.4528
	+90	0.3959	0.3959	0.3959	0.3959	0.3959	0.3959	0.3959	0.3959	0.3959	0.3959	0.3959	0.3959

Table 1. Magnitude of surface gravity (in  $\text{cm/s}^2$ ) as a function of latitude and longitude.

Figure 3 shows the Phobos orbital frame, and Figure 4 shows the result of simulations with descent trajectories from a distribution of initial conditions, which take into account the complex gravitational model of Phobos and the tidal (three-body) effects from Mars. Table 1 shows the magnitude of surface gravity as a function of latitude and longitude. Other concepts would require that an astronaut performs extra-vehicular activity and move on and around the surface of Phobos to collect samples or emplace assets useful for further exploration. Such situations would require effective locomotion mechanisms in a low-gravity environment, where the interaction forces (examples of which are shown in Figure 5) would be dominated by interaction with the surface soil layers, due to the low gravity levels.

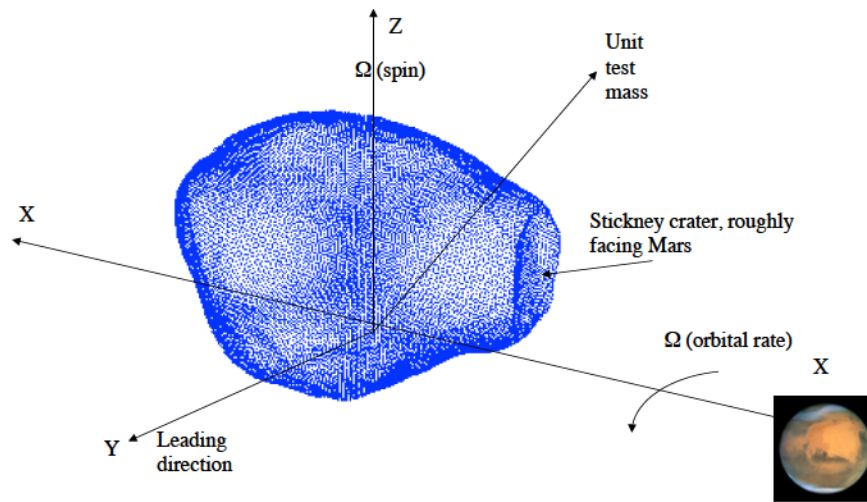


Figure 3. Phobos orbital frame.

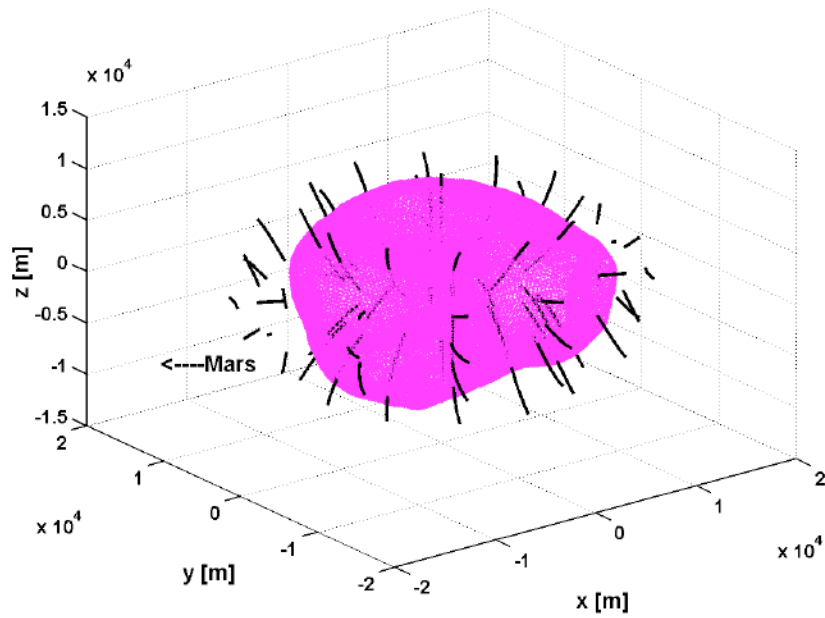


Figure 4. Descent trajectories from a distribution of initial conditions.

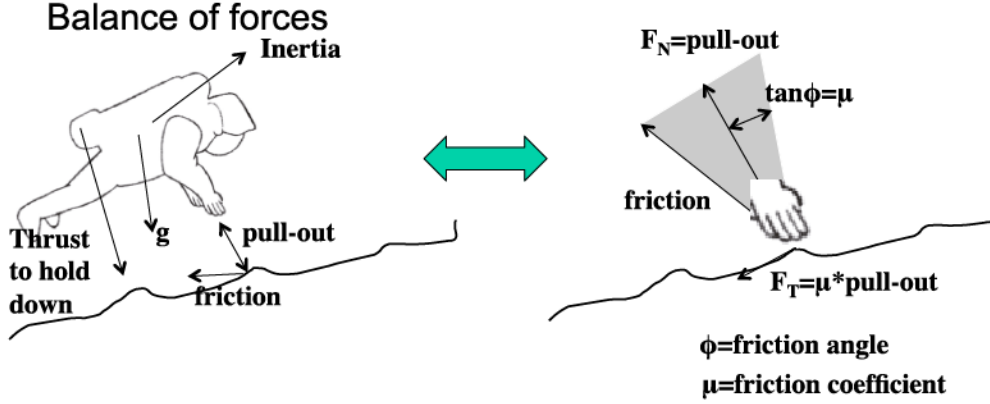


Figure 5. Balances of forces on astronaut interacting with Phobos' surface.

#### IV. Models for the interaction between the footpad and regolith material

As the performance of the hopper would be a function of its own electro-mechanical characteristics (e.g. mechanical springs, pad size) and the properties of the regolith, it is important to understand the physics of both models. To this end we examined the literature on such interaction models in order to determine hopper-relevant performance parameters (e.g. soil compliance) from more fundamental physical properties of the regolith. We also conducted simulation studies to better understand the physical models e.g. time constants, energy decay, etc.

Figure 6 shows the phases of soil interaction of an equivalent “pogo-stick” model that was used to conduct the analysis. To simplify the analysis we considered very simple prototype models of the vehicle during the hop (pogo-stick), and conducted a sensitivity analysis of how the soil parameters influence the hop at the footpad level. In the investigation of the soil interaction during the hop, we found that the existing models are used quasi-statically, and are not really applicable to the highly dynamic soil interaction event that takes place during a hop. Previous models used for anchoring simulations and for wheel-soil interactions were shown to be inadequate. While it is known that carbonaceous chondrites abound on the surface of Phobos, data on the soil properties at the surface of Phobos is also very scarce, if it exists at all. Also, we found that all the existing soil models are macroscopic, following soil failure criteria such as the Mohr-Coulomb model, and that there exists no existing mapping between the parameters in the soil failure model and the microscopic soil properties (Young's and Shear modulus, Poisson's ratio, cohesion) that can be measured via remote sensing. This lack of data indicates that tests should be done to determine these parameters. To verify the soil contact models, comparisons were made with the canonical bouncing ball model [Azad et al.]. Three soil-interaction models were exercised. In the first model [Anderson et al., Balaram et al., Quadrelli et al.], the penetration model used in previous anchoring work was used. This was a one-dimensional penetration model suitable for highly dynamic transient events. The second model was a terramechanics model used for rover locomotion [Ding et al., Liang et al], typically used in quasi-static penetration conditions. This interaction model, shown in Figure 7 (taken from Liang), is given by the following equations:

$$\begin{aligned}
 F_n &= \sigma S \\
 F_t &= \tau S \\
 \sigma(\delta) &= (k_c / b + k_\phi) \delta^n \\
 \tau(\delta) &= (c + \sigma \tan \phi)(1 - e^{-j/K})
 \end{aligned} \tag{2}$$

where  $F_n$  is the normal force,  $F_t$  is the tangential force,  $S$  is the contact area,  $\sigma$  is the normal stress,  $\tau$  is the tangential stress,  $c$  is the soil cohesion parameter,  $\phi$  is the soil angle of friction,  $j$  is the tangential penetration, and  $K$ ,  $k_c$  and  $k_\phi$  are soil parameters shown in Table 2, taken from [Zhou].

The third model was a Hunt-Crossley model with Lysmer analog [Richart], which turned out to be ideal for the hopper simulation as in effect it is an equivalent spring-damper model. Contrary to conventional Kelvin-Voigt

models (of the form  $F = kx + c\dot{x}$ ), which suffer from the fact that start and end with discontinuity, and also that the force can take negative values even if it is not a sticky or tensile terrain, the Hunt-Crossley model is of the form  $F = kx^n + c\dot{x}^n$ , is usually used with  $n = 3/2$  to resemble a Hertzian contact, and has been experimentally proven as a robust model for viscoelastic impacts. Therefore, given the soil constants ( $G$ =shear strength, density  $\rho$ , and Poisson's ratio  $\nu$ ), the equivalent stiffness  $K$  and damping  $C$  coefficients are:  $K = \frac{4Gr_0}{1-\nu}$  and  $C = \frac{3.4r_0^2}{1-\nu}\sqrt{\rho G}$ , where  $r_0$  is the radius of the footpad. The normal and tangential force models are then:

$$\begin{aligned} F_n &= (K + C\dot{\delta})\delta^{3/2} \\ F_t &= -\mu \cdot \text{sign}(V_{rel})|F_n| \end{aligned} \quad (2)$$

where  $\delta$  is the penetration depth,  $\mu$  is the Coulomb friction coefficient, and  $V_{rel}$  is the relative tangential velocity at the point of contact. These models were tested with a single rigid body falling on ground and with a pogo-stick model, with two rigid bodies connected by a spring and a damper with translation joint + control. The conclusions of the first model (shown in Figure 5) are that, for the trajectory during the hop, the system restitution was dominated by spring at leg, was independent of soil density, while soil cohesion and friction angle displayed a delay effect (hysteresis) on the hop.

Figure 8 shows the results of the footpad-soil interaction simulation varying density, angle of friction, and cohesion. Figure 9 shows the results of footpad-soil interaction simulation for a jump from static rest, showing the hysteretic force-displacement curve, and the velocity ( $\Delta V$ ) reached by the top mass. Figure 10 shows the results of footpad-soil interaction simulation for the following conditions:  $V_z=0$  m/s;  $V_x=0.025$  m/s;  $\mu=0$ . Figure 11 shows the results of footpad-soil interaction simulation for the following conditions:  $V_z=-0.5$  m/s;  $V_x=0.025$  m/s;  $\mu=0.6$ . Figures 12 and 13 show the results of footpad-soil interaction simulation varying leg spring stiffness and dissipation coefficients. Figures 14, 15, and 16 show the results of the simulation of the hop from rest, also varying spring stiffness and dissipation parameters. The conclusions of model led to the observation that control forces and torques are needed to cancel the effect of the tangential force induced by friction. The third model was more promising than the other two models, as it was able to capture impact and restitution for a wide range of soil properties. Simulation results are shown in Figures 8 through 16, for the case in which the vehicle jumps from rest conditions, showing that, with attitude control, the  $\Delta V$  that can be achieved at the end of the jump is approximately 0.5 m/s. It was also observed that it remains unclear yet how to go from soil ab-initio parameters ( $G$ ,  $\nu$ ) to parameters of soil bearing strength model (cohesion, friction angle). The main conclusion of the simulations is that the magnitude of the  $\Delta V$  during the bounce (the equivalent coefficient of restitution of the system) would be dominated by the spring and damper parameters at the leg, and much less by the equivalent spring and damper parameters modeling the soil. For the simple pogo-stick model, the friction forces at the foot would be destabilizing (vault pole problem), and would require a combination of attitude and translation control to redirect the vehicle to the next jump.

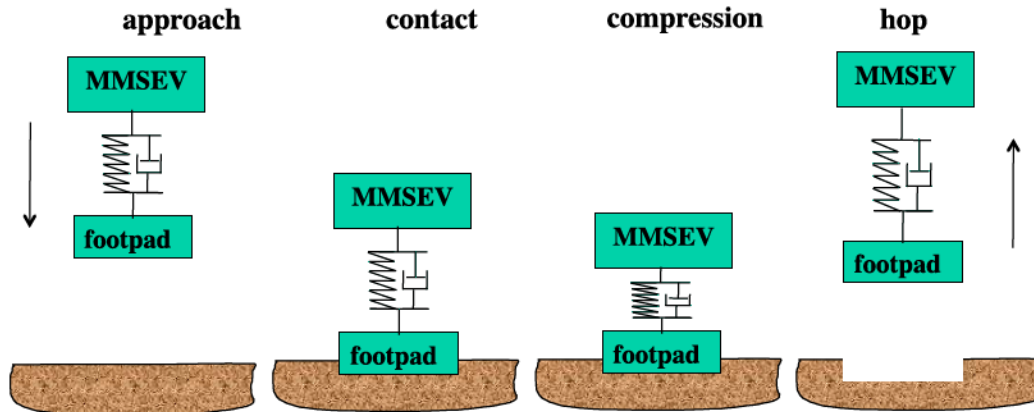


Figure 6. Footpad-soil interaction model.

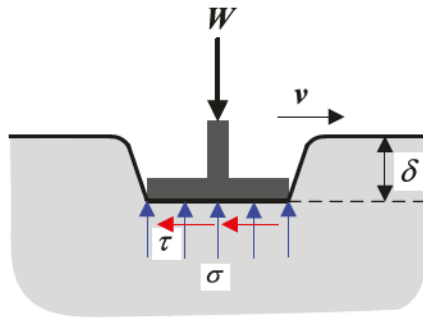


Figure 7. Soil pad stress interaction model used in this paper, taken from [Liang].

Table I. Measured and estimated Mars Mojave Simulant soil parameters.

	$\rho$	$c$	$\phi$	$k'_c$	$k'_\phi$	$n(n_0)$	$n_1$	$k_x$	$a_1$	$a_2$	Rebound
units	kg/m <sup>3</sup>	kPa	deg	-	-	-	-	mm	-	-	-
Starting values	1550	0.6	35	677.5	212.2	1.4	0.54	0.6	0.33	0.11	3%
Final values	1550	0.6	35	677.5	212.2	1.4	0.354	14.6	0.365	0.503	7%

#31

Table II. Soil parameters for modeling SSTB-Lite Dumont Dunes tests.

	$\rho$	$c$	$\phi$	$k'_c$	$k'_\phi$	$n(n_0)$	$n_1$	$k_x$	$a_1$	$a_2$	Rebound
unit	kg/m <sup>3</sup>	kPa	deg	-	-	-	-	mm	-	-	-
initial	1650	0.2	30	677.5	212.2	1.4	0.37	12	0.33*	0.11*	5%
final	1650	0.2	30	9.1	500.8	1.4	0.45	29	0.33*	0.11*	5%

#32

Table III. Estimated parameters for multiple soil simulation on Sol 2143.

soil	$\rho$	$c$	$\phi$	$k'_c$	$k'_\phi$	$n_0$	$n_1$	$k_x$	$a_1$	$a_2$	$k_1$	$k_2$
unit	kg/m <sup>3</sup>	kPa	deg	-	-	-	-	mm	-	-	-	-
1	1600	1.5	35	100	1000	1.1	0.1	15	0.33	0.11	1.154	0.0348
2	1300	0.25	30	10	300	1.4	0.18	25	0.32	0.20	1.154	0.0348
3	1600	2.5	35	100	1000	1.1	0.1	12	0.33	0.11	1.154	0.0348

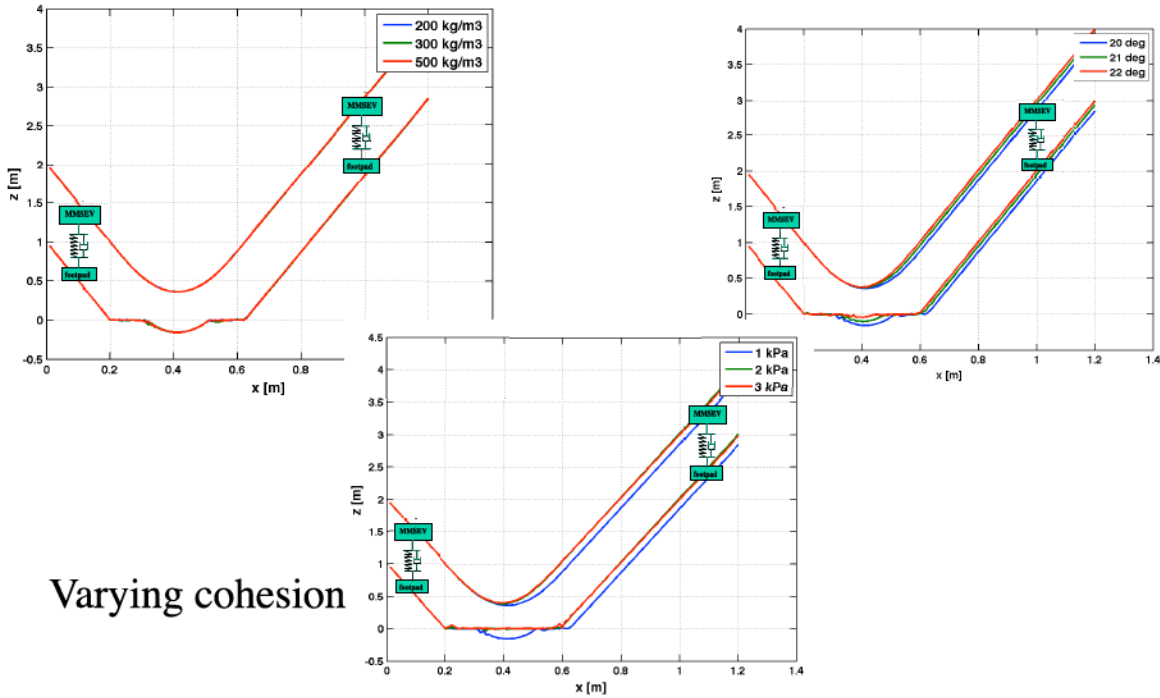
#3

Table IV. Bedrock friction parameters and nominal values.

Frictional parameters	Description	Unit	Nominal Value
$k$	material stiffness between wheel and bedrock	N/m <sup>6</sup>	7.53E+007
$e$	exponent of the force deformation characteristic	-	2.0
$c_{max}$	maximum damping coefficient between wheel and bedrock	kg/s	8140.0
$z_{max}$	maximum penetration	m	0.002
$\mu_s$	static friction coefficient between wheel and bedrock	-	0.757
$\mu_d$	dynamic friction coefficient between wheel and bedrock	-	0.597
$v_{st}$	stiction transition velocity	m/s	0.03
$v_{f1}$	friction transition velocity	m/s	0.05

Table 2. Soil parameters (31, 32, 3) used in this paper, taken from [Zhou].

## Varying density



## Varying cohesion

Figure 8. Results of footpad-soil interaction simulation varying density, angle of friction, and cohesion.

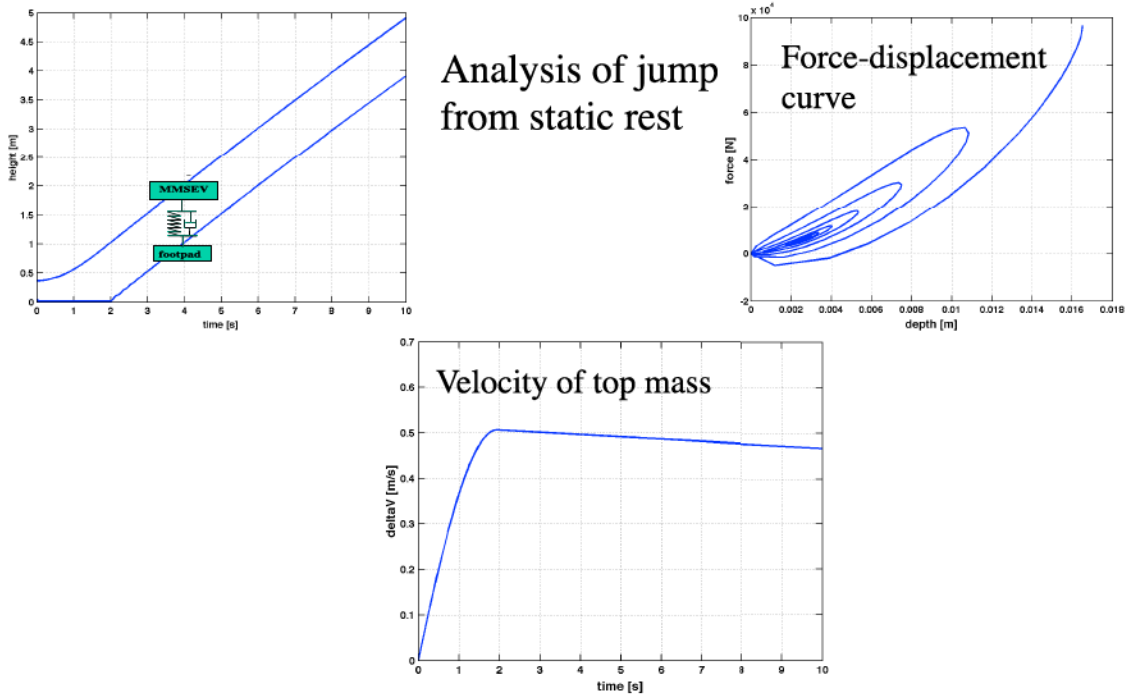


Figure 9. Results of footpad-soil interaction simulation for a jump from static rest, showing the hysteretic force-displacement curve, and the velocity ( $\text{delta}V$ ) reached by the top mass.

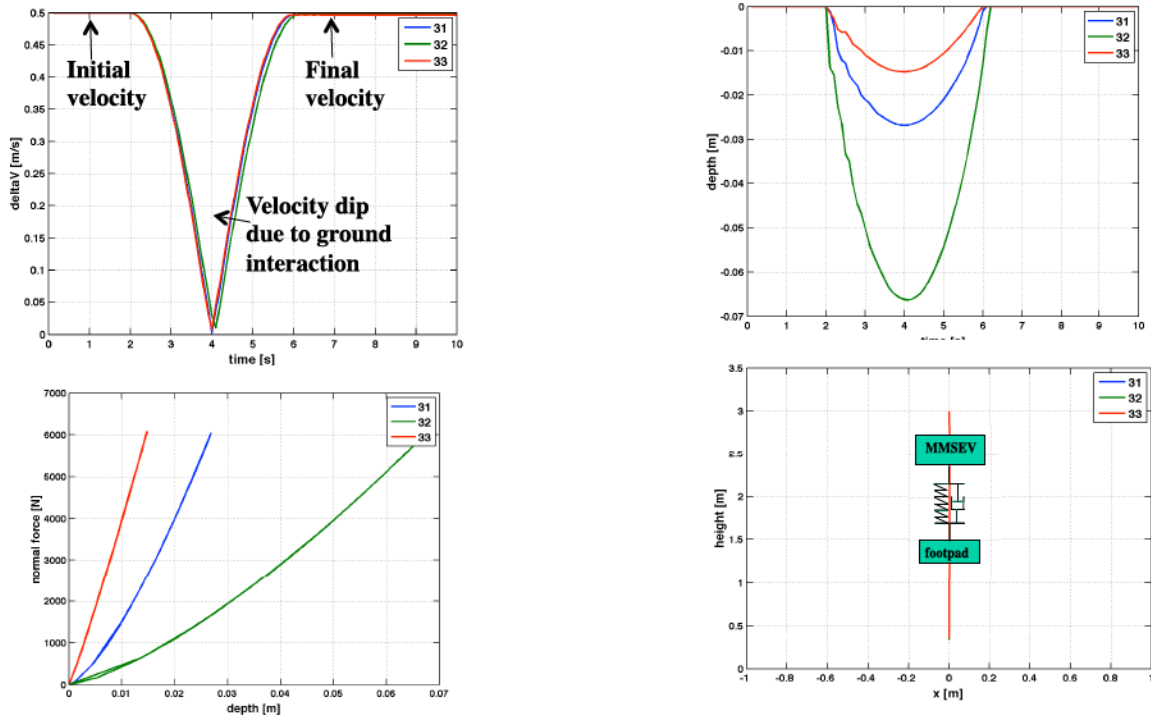


Figure 10. Results of footpad-soil interaction simulation:  $V_z=0$  m/s;  $V_x=0.025$  m.s;  $\mu=0$

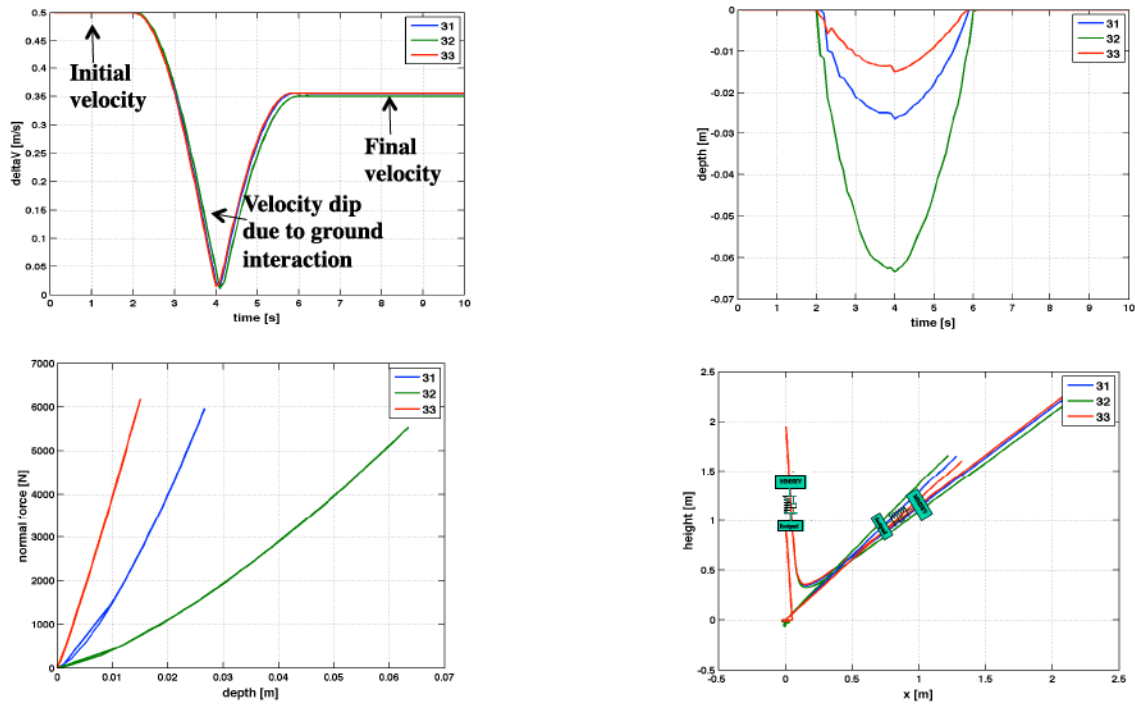


Figure 11. Results of footpad-soil interaction simulation:  $V_z=-0.5$  m/s;  $V_x=0.025$  m.s;  $\mu=0.6$

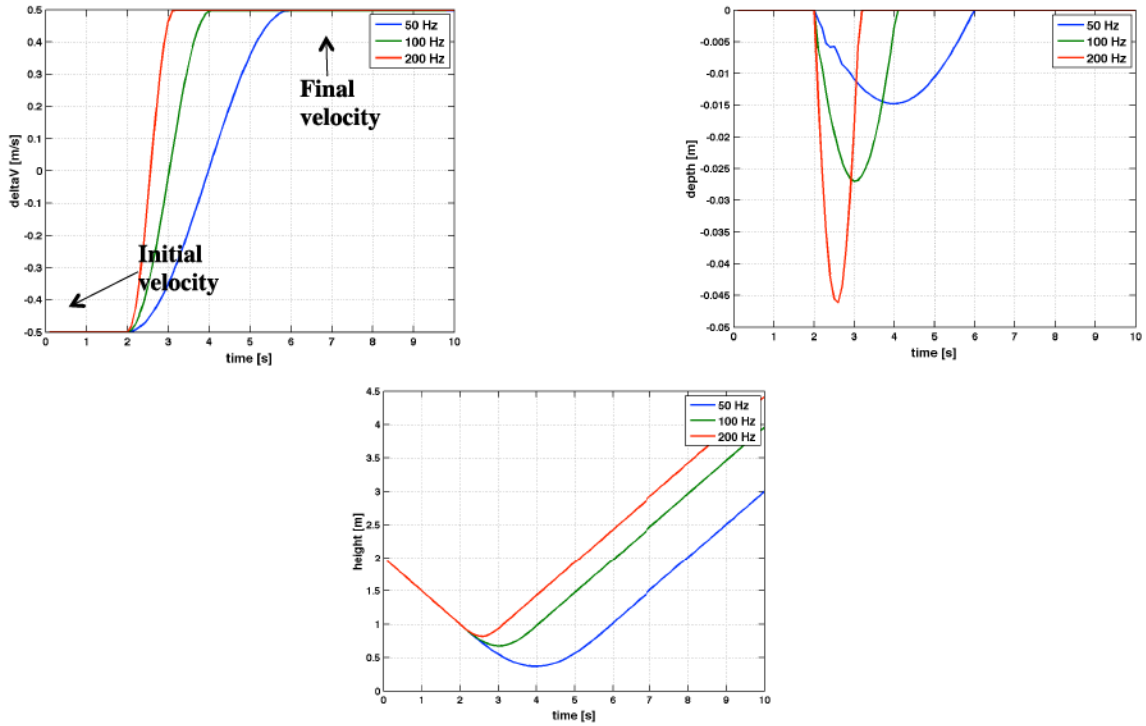


Figure 12. Results of footpad-soil interaction simulation: varying spring stiffness

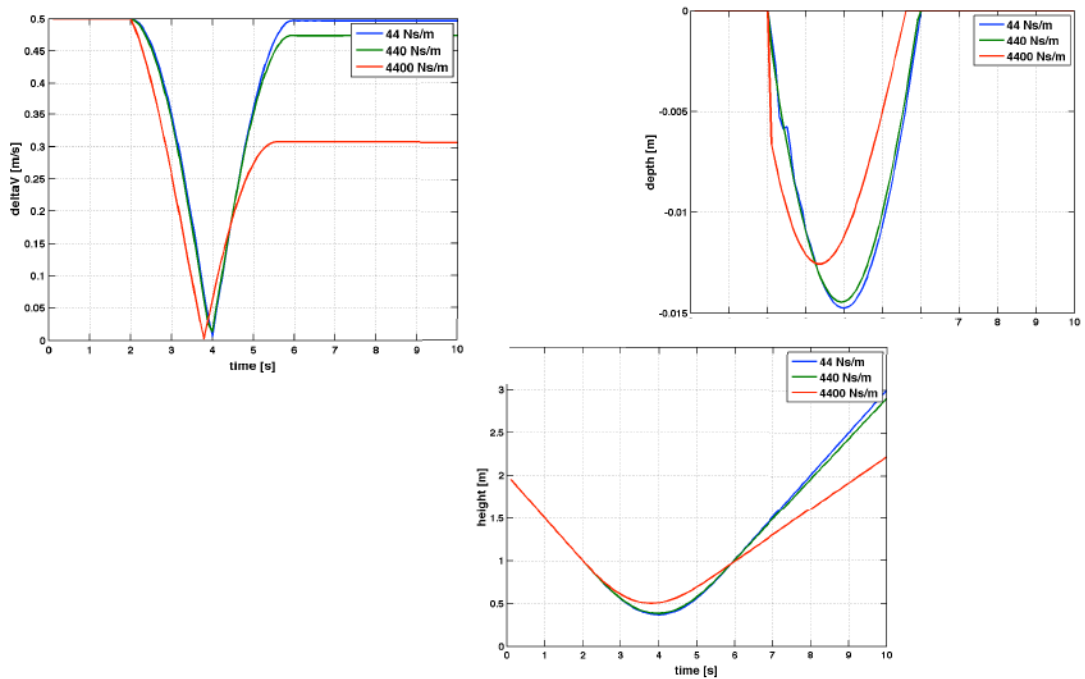


Figure 13. Results of footpad-soil interaction simulation: varying spring dissipation

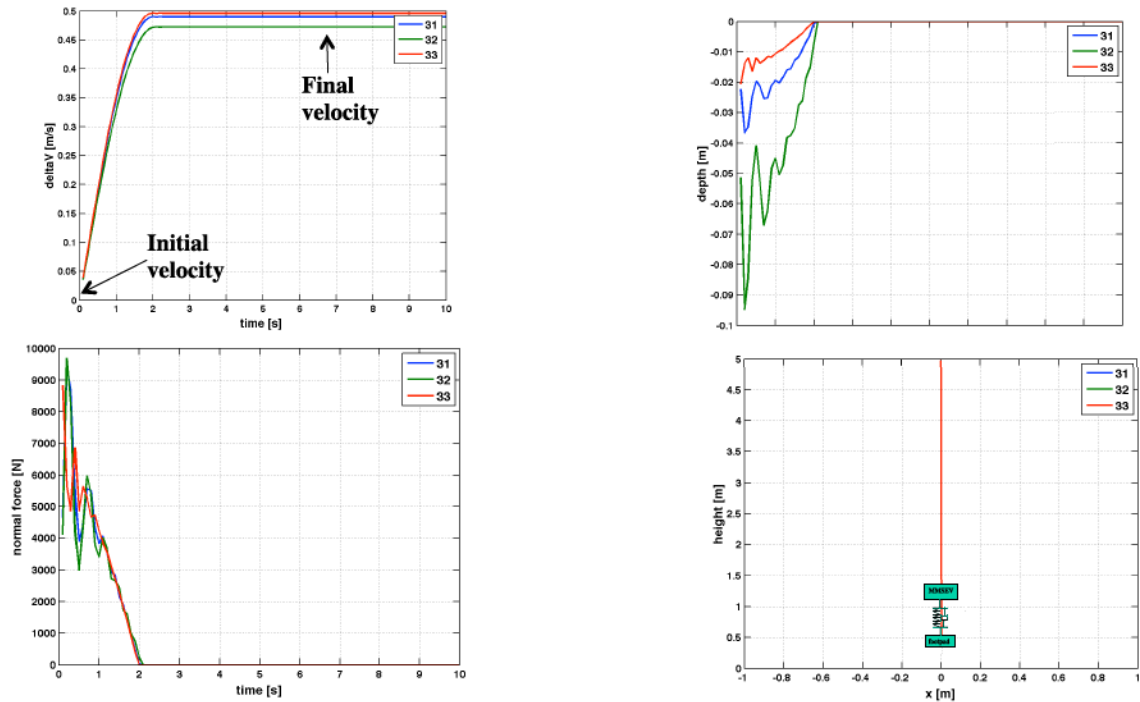


Figure 14. Results of footpad-soil interaction simulation: Hop from rest

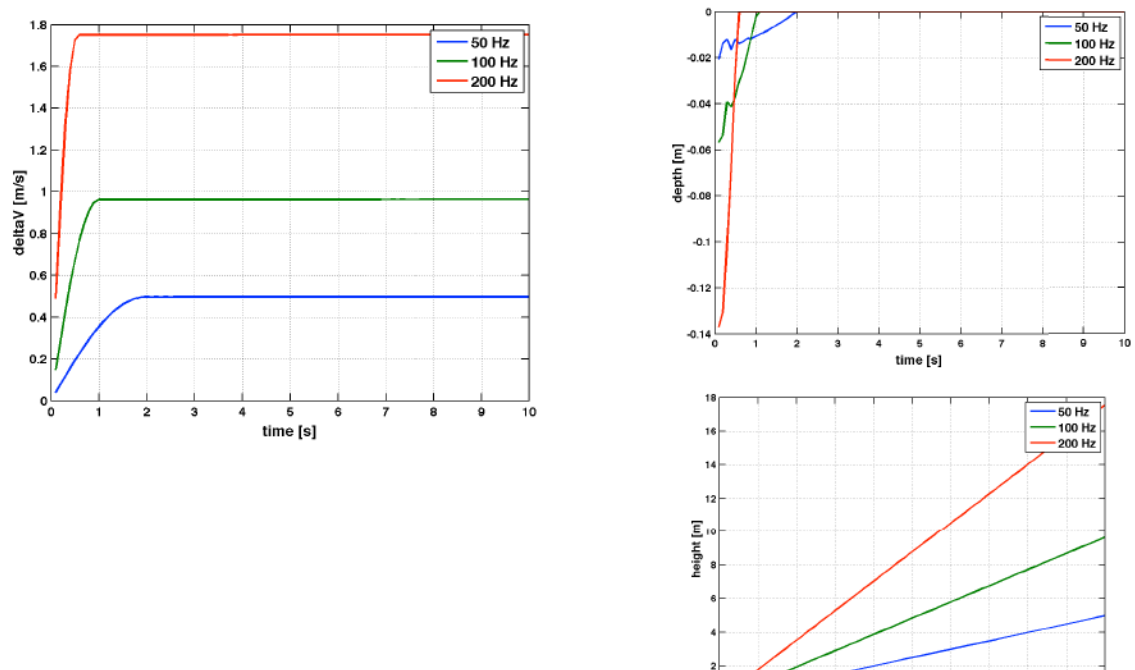


Figure 15. Results of footpad-soil interaction simulation: Hop from rest, varying spring stiffness

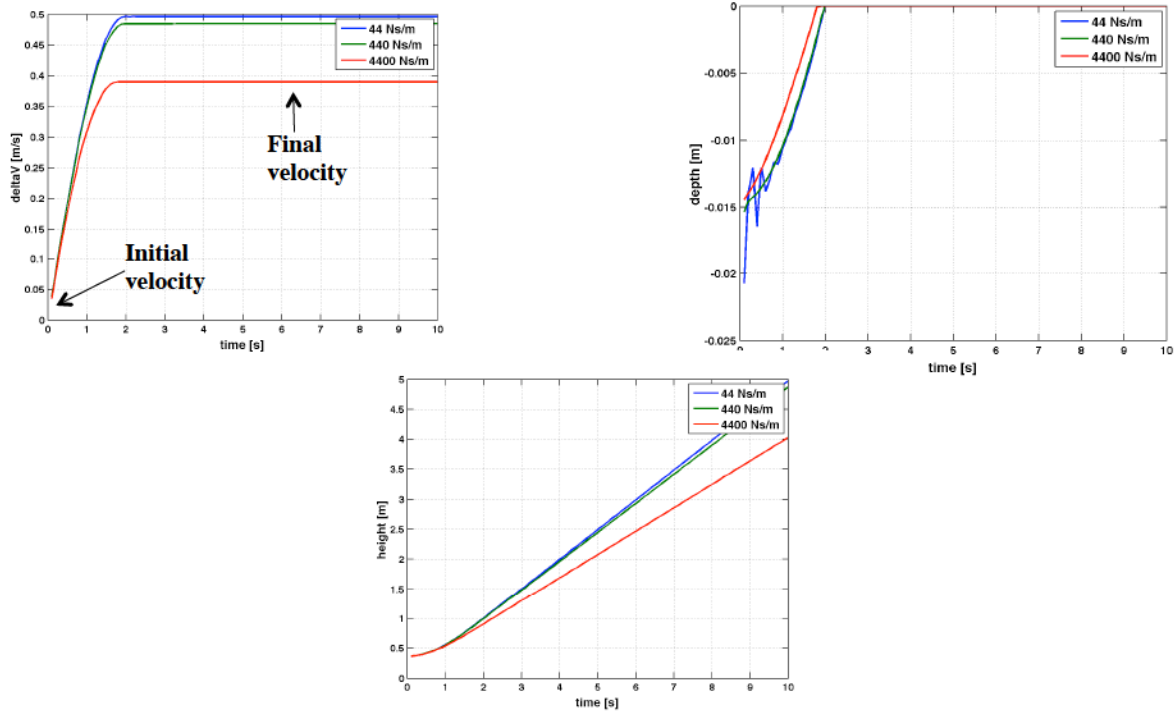


Figure 16. Results of footpad-soil interaction simulation: Hop from rest, varying spring dissipation

## V. System level effects relating to Hopper configuration geometry

The hop dynamics of the full-size articulated Athlete vehicle with the soil interaction modeled as an equivalent coefficient of restitution was also analyzed. The ability of the hopper to achieve a delta-V as it departs from the surface would be a function of the electro-mechanical system at each of the pads (springs, linear motors, etc.), the regolith properties, and the geometrical configuration of the contacting pads with the terrain. A hopper with vertical orientation on all legs operating on hard regolith would achieve the best performance. On the other hand, a hopper departing at an angle, with legs also at angles to the surface, operating on softer/looser regolith would not be able to achieve the same performance. In order to understand these geometric effects, we developed a dynamics simulation of an Athlete configuration vehicle, with simpler physics-based models (coefficients of restitution and friction) for the foot-terrain interaction. We have conducted some initial parametric analysis of this system to analyze both (i) departure delta-V performance as a function of geometry, and (ii) energy dissipation and settling times for passive hops at different approach angles. Since the original Athlete vehicle models would have wheels and would have no springs on the legs, the vehicle model needed to be updated to be representative of the new vehicle for Phobos. Simulations runs have been carried out varying the equivalent coefficient of restitution at the ground contact point, the horizontal and vertical components of the approach velocity, and the vehicle body rates. The simulations identify ranges of parameters for which the vehicle emerges stably (relying only on the passive viscoelastic damper at each leg) or unstably (needing active attitude control) from the hop.

We simulated a wide range of landing conditions for a 1 meter high drop, varying initial conditions and parameters, on flat, featureless, non-compliant ground, and used a canonical short distance hop to study the effects of footpad-ground interaction (results can be extrapolated larger hops). The simulation runs were done for 50 seconds of motion for various cases: a) varied vertical velocity from 0.1 - 0.5 m/s in steps of 0.1 m/s ; b) Varied horizontal velocity from 0.01 - 0.05 m/s in steps of 0.01 m/s; c) coefficient of restitution varied: 0.1, 0.25, 0.5, and 0.9. d) Coefficient of friction = 0.1 to 0.9. In all cases, the Leg spring constant was 8883 N/m, the Damping constant was 396 N\*s/m, and the assumed value of Gravitational acceleration = 0.05 m/s<sup>2</sup> (Phobos-normal). Figure 17 shows the summary of the results of this hopping simulation. Circle size corresponds to coefficient of restitution (larger diameter = larger coefficient). Circle color corresponds to hopper energy after 50s (measured as kinetic energy of chassis plus the

potential energy in each of the six springs). The buckets are:  $< 1.0$  kJ = black;  $1.0\text{kJ} - 1.5\text{kJ}$  = red;  $1.5\text{kJ} - 2.0\text{kJ}$  = blue;  $2.0\text{kJ} - 2.5\text{kJ}$  = green;  $> 2.5\text{kJ}$  = magenta. Figure 18 shows the results of the validation of hopping simulation for three cases with all joints locked (infinitely rigid vehicle): elastic bounce for vertical drop, pure horizontal sliding, pure plastic sticking at maximum ground friction coefficient. Figure 19, 20, and 21 show the horizontal position, vertical position, and angle from vertical of the leg tips as function of ground friction coefficient ( $\mu$ ) and restitution coefficient ( $e$ ). Further assessments on the vehicle stability and attitude control would require the development of control logic to stop the vehicle from bouncing once in contact with the ground, or to keep the vehicle stable in flight when it jumps off the surface.

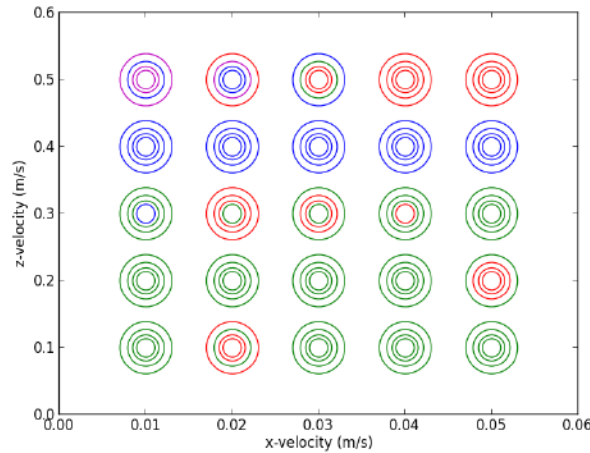


Figure 17. Results of hopping simulation. Circle size corresponds to coefficient of restitution (larger diameter = larger coefficient). Circle color corresponds to hopper energy after 50s (measured as kinetic energy of chassis plus the potential energy in each of the six springs). The buckets are:  $< 1.0$  kJ = black;  $1.0\text{kJ} - 1.5\text{kJ}$  = red;  $1.5\text{kJ} - 2.0\text{kJ}$  = blue;  $2.0\text{kJ} - 2.5\text{kJ}$  = green;  $> 2.5\text{kJ}$  = magenta.

### Infinitely rigid leg spring (rigid vehicle)

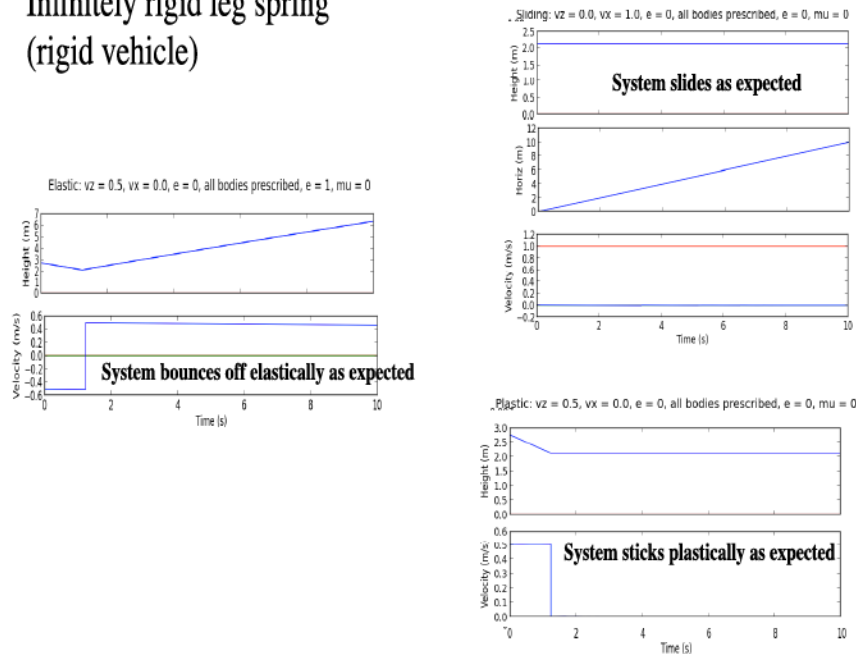


Figure 18. Results of validation of hopping simulation for three cases with all joints locked (infinitely rigid vehicle): elastic bounce for vertical drop, pure horizontal sliding, pure plastic sticking at maximum ground friction coefficient.

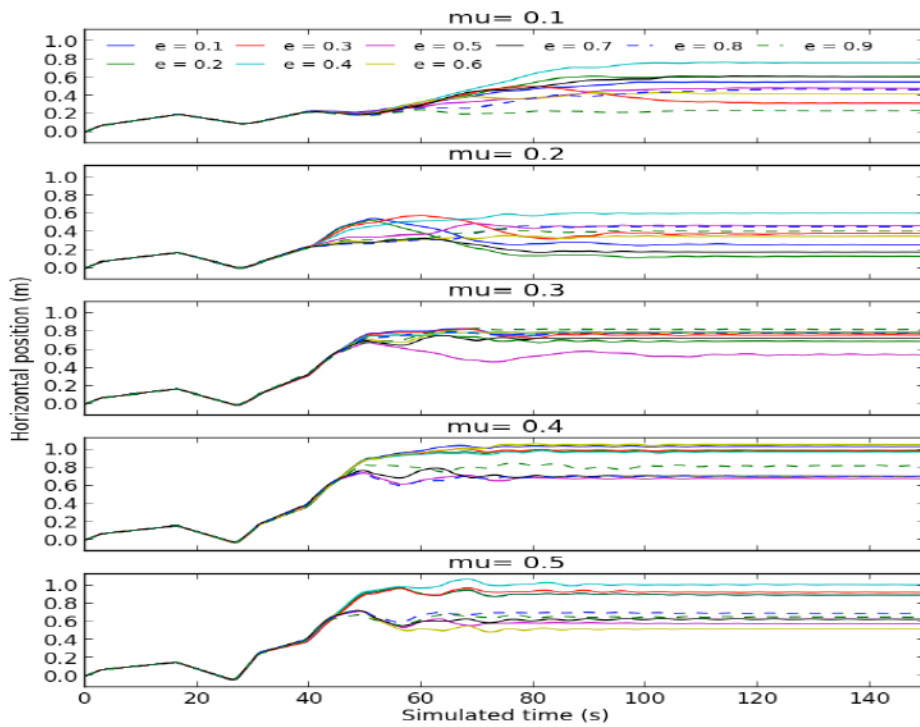


Figure 19. Horizontal position of leg tips as function of ground friction coefficient ( $\mu$ ) and restitution coefficient ( $e$ ).

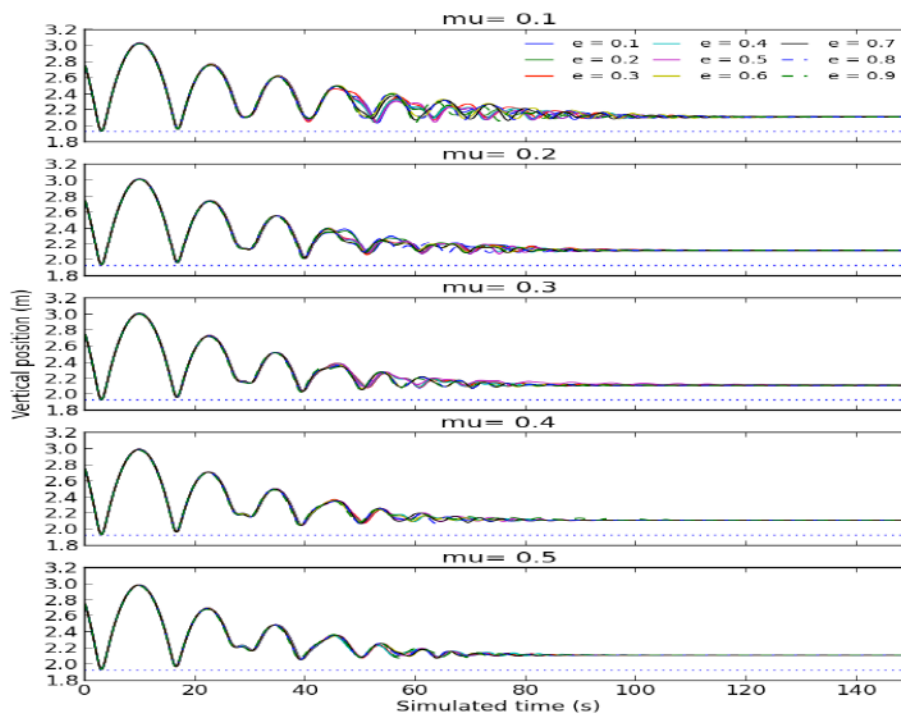


Figure 20. Vertical position of leg tips as function of ground friction coefficient ( $\mu$ ) and restitution coefficient ( $e$ ).

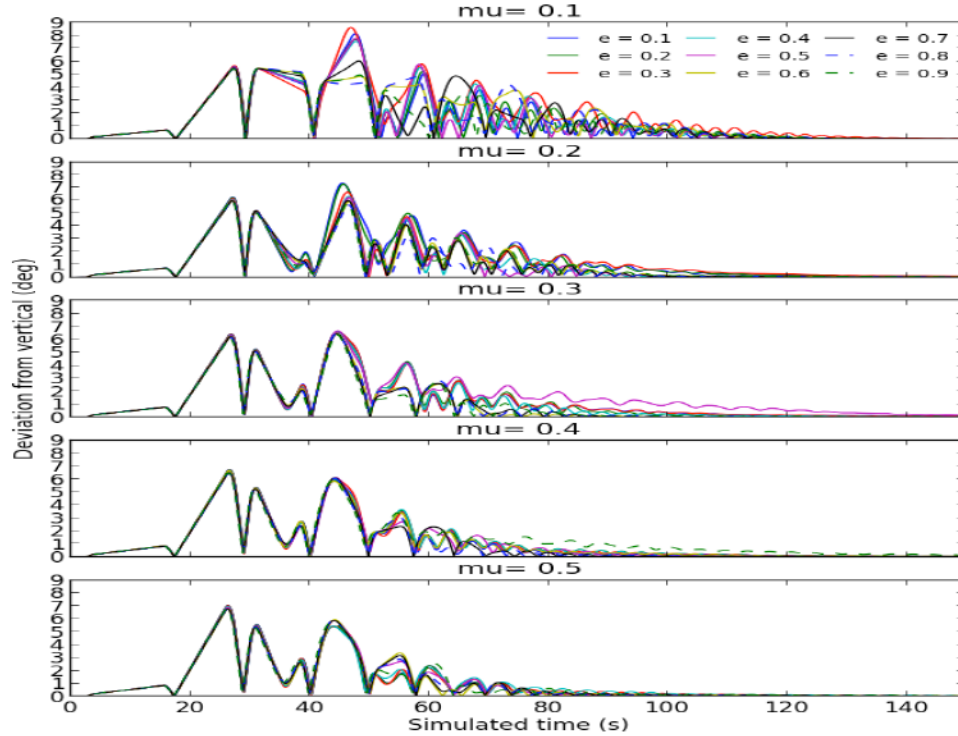


Figure 21. Angle from vertical of leg tips as function of ground friction coefficient ( $\mu$ ) and restitution coefficient ( $e$ ).

## VI. Conclusions

In conclusion, we have analyzed the dynamics of a spacecraft in proximity of Phobos by developing the equations of motion of a test mass in the Phobos rotating frame using a model based on circularly-restricted three body problem, and by analyzing the dynamics of a hopper vehicle interacting with the soil. The simulated trajectories showed different deviations toward Mars depending on the initial lat-long and height. The results of the footpad-soil interaction study indicate that there are currently no satisfactory models that capture the interaction physics and which are traceable to particular properties of various regions on Phobos. Also, the results of the hopping performance study indicate that: a) the system restitution is largely dominated by the spring at each leg; b) the soil properties effect on hopping  $\Delta V$  is very small; c) the effect of friction coefficient is large for large lateral velocities, requiring active control for stabilization. In the case of a jump from rest, the soil properties change the initial conditions, but the effect on the jump  $\Delta V$  is small compared to the effect of the leg spring. It is unclear yet how to go from soil ab-initio parameters to parameters of soil bearing strength model (cohesion, friction angle) and to coefficient of restitution. A vehicle system-level study was also conducted. Since the original Athlete vehicle models had wheels and had no springs on the legs, the vehicle model needed to be updated to be representative of the new vehicle for Phobos. Simulations runs have been carried out varying the equivalent coefficient of restitution and coefficient of friction at the ground contact points, the horizontal and vertical components of the approach velocity, and the vehicle angular body rates. The simulations identify ranges of parameters for which the vehicle emerges stably (relying only on the passive viscoelastic damper at each leg) or unstably (needing active attitude control) from the hop. The main conclusion of the numerical studies is that the system response is dominated by the stiffness and damping parameters of the leg springs, with the soil characteristics having a much smaller effect. The implication is that further experimental and possibly computational modeling work, as well as site characterization (from precursor missions) will be necessary to obtain validated performance models. The system simulations identify ranges of parameters for which the vehicle emerges stably (relying only on the passive viscoelastic damper at each leg) or unstably (needing active attitude control) from the hop. Future work would be done to improve the Phobos-detic/Phobos-centric mapping to assist in more precise surface dynamics simulations, and carry out

sensitivity studies of astronaut performance by means of simulations of astronaut locomotion on surface. Additional parametric studies would need to be conducted on achievable hopper delta-V with non-flat terrain and conforming feet. Parametric trades related to unwanted moments and required control authority from thrusters and/or control-moment gyros (CMGs) would also be needed in future studies.

## References

- Anderson et al.: *Penetrator Emplacement into Planetary Surfaces*, Journal of Geophysical Research, vol. 101, no. E9, pp.212, 137-21, 149, September 25, 1996.
- Azad, M., and Featherstone, R.: *Modelling the Contact between a Rolling Sphere and a Compliant Ground Plane*, Australasian Conf. Robotics and Automation (ACRA 2010), Brisbane, Australia, 1-3 December 2010.
- Balaram et al., *Physics-Based Simulator for NEO Exploration Analysis and Modeling*, presented at AIAA SPACE 2011 Conference and Exposition, Long Beach, California, Sep. 27-29, 2011.
- Castillo, J.: *Phobos and Deimos, state of knowledge in preparation for future exploration*, presentation at Initial Phobos/Deimos DRM meeting for HAT, Caltech Space Challenge, 2013, <http://csc.caltech.edu>.
- Davis, et al: *The Unusual Dynamical Environment of Phobos and Deimos*, Icarus, 47, 1981, pp. 220-233.
- Ding, L., et al: *Foot-terrain interaction mechanics for legged robots: Modeling and experimental validation*, The International Journal of Robotics Research 2013 32: 1585.
- Dobrowolskis, Burns: *Life near the Roche Limit: behavior of ejecta from satellites close to planets*, Icarus, 42, 1980, pp. 422-441.
- Duxbury, T.: *The Figure of Phobos*, Icarus, 78, 1989, pp. 169-180.
- Liang et al: *Foot-terrain interaction mechanics for legged robots: Modeling and experimental validation*, The International Journal of Robotics Research 2013 32: 1585.
- Quadrelli, M., Mazhar, H., Negrut, D.: *Modeling and Simulation of Anchoring Processes for Small Body Exploration*, AIAA SPACE 2012 paper. AIAA2012-5310.
- Richart, F.E.: *Vibrations of Soils and Foundations*, Prentice-Hall, 1970.
- Thomas et al, *Phobos: regolith and ejecta blocks investigated with Mars Orbiter Camera Images*, JGR, co. 105, no. E6, pp. 15091-15106, June 25, 2000.
- Zhou et al.: *Simulations of Mars Rover Traverses*, Journal of Field Robotics, 31(1), 141-160, 2014.